Multi-Objective Optimization Algorithm of Humanoid Robot Walking on a Narrow Beam

Kittisak Sanprasit
Department of Electrical and Electronic Engineering, Faculty of Industrial Technology, Loei Rajabhat University, Loei, Thailand
Email: kittisak.san@lru.ac.th

***Abstract*— The humanoid robots associate and work with human, they should be able to access anywhere people can even in complex and harsh environments. This research proposes an optimal path design for humanoid robots to walk on a narrow beam. The experiments and simulations of a commercial humanoid robot (Bioloid Premium Type A), with 18 Degree of Freedoms (DOFs) were conducted. The multi-objective optimization was used to design the walking path of the robots on the beam by comparing four algorithms: MOWOA, MOGWO, MOHS, and MOGA. The performance comparison was made based on the hypervolume (HV) indicator. The optimal points were chosen from non-dominated solutions by MCDM method and minimization weighted sum method (WSM). There were two objective functions: 1) maximum postural stability of a humanoid robot walk and 2) minimal jerk.**

***Index Terms*— humanoid robot, MOWOA, MOGWO, MOHS, MOGA, weighted sum method, hypervolume, Pareto front**

I. Introduction

The main goal of humanoid robot development is that they can work cooperatively with humans [1]. Therefore, the humanoid robot should be able to access anywhere people can, even in complex and harsh environments. The humanoid robots should be able to work where people work such as stairs [2], slopes [3], and stepping-stones [4]. Walking, jumping and running [5-8] have been fundamental research topics in the field. The main problem is to maintain robust balance while walking because the robots have complex and non-linear systems, and hard-to-stabilize dynamic poses.

To keep the balance on the beams, humans need to control their bodies very well so they can transport and complete their mission on such a dangerous area as balance beam without falling. In general, there are two types of stability criteria that the trajectories of a biped mechanism depend on: static stability and dynamic stability. Static stability requires vertical projection of the center of mass (COM) of the robot within the support polygon (SP) formed by its two feet [6]. Walking on the beam is difficult because the support area is narrow. Therefore, the robot needs a stable and accurate control system.

Enrico Chiovetto et al. [9] studied human walking on a beam by rotating the limb segments to control the body's angular momentum. Participant walked on a narrow beam and wore the marker sets for 3D kinematic data acquisition. David E.Orin, Ambarish Goswami, and Sung-Hee Lee [10] present the COM of a humanoid robot occupies a special place in its dynamics. They specifically studied the properties, structures and computation schemes for the centroidal momentum matrix (CMM), and introduced the new concept of "average spatial velocity". The momentum-based balance was controlled by simulating a humanoid robot model inside the width of the support beam. Robert J et al. [11] present a new footstep planner that utilizes a planar region representation of the environment enable footstep planning over rough terrain. They demonstrate this planner over a variety of virtual and real world environments, including some that require partial footholds, rough terrain, and narrow beam. In other previous studies, walking gait methods on a balance beam often require complex mathematical models.

This paper designs walking trajectory on a narrow beam and minimizes jerk to prevent damage from joint equipment by meta-heuristic algorithm which is a popular technique because of its simplicity. We present the humanoid robot and the pre-defined humanoid robot walking gait in the simulations and experiments. The simulation develops kinematics humanoid robot by MATLAB. It calculated COM, SP, and the jerk of joint. This work also proposes a multi-objective optimization to determine how the humanoid robot walks on a narrow beam. Two objective functions were employed: maximum postural stability of the walk and the minimum jerk of a humanoid robot. We compares multi-objective meta-heuristics (MOMHs) [12] for optimum design of a humanoid robot walking on a narrow beam. The optimizers use four algorithms: Multi-objective Whale optimization Algorithm (MOWOA) [13], Multi-objective Grey Wolf Optimizer (MOGWO) [13], Multi-objective Harmony Search Algorithm (MOHS) [14], and Multi-objective Genetic Algorithm (MOGA) [15]. The programs was developed by using MATLAB computing language. The non-dominated solution was used to find Pareto front. Various optimizers performance were compared based on hypervolume (HV) indicator [12, 13]. The minimal the weighted sum method (WSM) was used

Manuscript received March 7, 2020; revised October 19, 2020.

doi: 10.18178/ijmerr.9.12.1548-1559

to select the optimal point of Pareto front. The optimum point result was implemented on the real humanoid robot as an experiment to compare between the trial-and-error result and the actual one.

This paper starts with an introduction and followed by the humanoid robot modeling in Section 2. In Section3, the numerical simulation is explained, then the experimental results are shown in Section 4. Finally, the conclusion is made in Section 5.

II. Humanoid Robot Modeling

In this section, we describe how to model humanoid walking on a narrow beam to be used in optimal control problem formulations. We start by describing the properties of the humanoid robot Bioloid premium Type A used in this study. Each link has its center of mass (Pcomi). The robot has 11 parts (i=1,2,..,11): ankle mass (M1), right knee mass (M2), right hip mass (M3), left hip mass (M4), left knee mass (M5), left ankle mass (M6), upper body mass (M7), right shoulder joint mass (M8), right elbow mass (M9), left shoulder joint mass (M10), and left elbow mass (M11), as shown in Fig. A in Appendix A. Appendix B shows the values of variables. The relationship between the position and attitude of a link and the joint angles of a mechanism called kinematics was made, and the movement of each frame for each joint was calculated by applying homogeneous transformation.

A. Kinematics Model

The kinematics consisted of 2 types which are 1) forward kinematics or direct kinematics and 2) inverse kinematics [16]. In 2012, J. Victor Nunez [17] invented inverse kinematics of 18 joints. A model of the robot developed from the Computer Aided Design (CAD) model provided by the manufacturer ROBOTIS. In 2013, Khairuddin Omar et al. [18] developed forward kinematics of 12 joints, considering only the legs, since it used for the gait cycle analysis for soccer robot competition FIFA 2013.

B. Forward Kinematics

In this research, the forward kinematics problem is the relationship between the operational coordinates of a robot on the Cartesian coordinate frame (x, y, z). It can analyze the stability of the robot. The forward kinematics use Denavit-Hartenberg (DH) [16]. A DH coordinate frame is defined by four parameters: θ_i, d_i, a_i, and α_i represents of joint angle, joint distance, link length, and link twist, respectively. All variables in each frame created as a table called "DH parameter table". It's reference parameter robot shown in Appendix A.

TABLE I. DH Parameter Table from Point Joint Left Ankle (V) to End Effector of Left Heel (F)

Frame No.	θ_i	d_i	a_i	α_i
1	q_1	0	0	-pi/2
2	q_2+$q_{i2,3}$	0	RL2	0
3	q_3-$q_{i3,4}$	0	RL3	0
4	q_4+$q_{i4,5}$	0	0	pi/2
5	q_5	0	RL4	pi/2
6	pi/2	0	0	-pi/2
7	q_6-pi/2	0	-RL5	0
8	q_7	LL4	0	pi/2
9	q_8+pi/2	0	0	-pi/2
10	q_9-$q_{i9,10}$	0	LL3	0
11	q_{10}+$q_{i10,11}$	0	LL2	0
12	q_{11}-$q_{i11,12}$	0	0	pi/2
13	q_{12}	0	LL1	0
14	0	LF2	0	0

TABLE II. DH Parameter Table from Center of Body (torso) to Point Effector of Right Hand (R)

Frame No.	θ_i	d_i	a_i	α_i
15	0	0	0	pi/2
16	pi/2	0	0	pi/2
17	0	D1	0	0
18	q_{13}	D2	D3	pi/2
19	q_{14}	0	D4	0
20	q_{15}	0	D5	0

TABLE III. DH Parameter Table from Center of Body (torso) to Point Effector of Left Hand (L)

Frame No.	θ_i	d_i	a_i	α_i
21	0	0	0	pi/2
22	pi/2	0	0	pi/2
23	0	-A1	0	0
24	q_{16}	-A2	A3	pi/2
25	q_{17}	0	A4	0
26	q_{18}	0	A5	0

C. Homogeneous Transformation Matrix

The DH parameter table used to calculate the movement of each frame for each joint by applying a homogeneous transformation matrix (1) to explain the rotation and sliding of each link according to the equation as follows [12].

$$
\begin{aligned}
{}^{i-1}T_i &= Rot_{z,\theta_i} Trans_{z,d_i} Trans_{x,a_i} Rot_{x,\alpha_i} \\
&= \begin{bmatrix} c_{\theta_i} & -s_{\theta_i} & 0 & 0 \\ s_{\theta_i} & c_{\theta_i} & 0 & 0 \\ 0 & 0 & 1 & 0 \\ 0 & 0 & 0 & 1 \end{bmatrix} \begin{bmatrix} 1 & 0 & 0 & 0 \\ 0 & 1 & 0 & 0 \\ 0 & 0 & 1 & d_i \\ 0 & 0 & 0 & 1 \end{bmatrix} \begin{bmatrix} 1 & 0 & 0 & a_i \\ 0 & 1 & 0 & 0 \\ 0 & 0 & 1 & 0 \\ 0 & 0 & 0 & 1 \end{bmatrix} \begin{bmatrix} 1 & 0 & 0 & 0 \\ 0 & c_{\alpha_i} & -s_{\alpha_i} & 0 \\ 0 & s_{\alpha_i} & c_{\alpha_i} & 0 \\ 0 & 0 & 0 & 1 \end{bmatrix} \quad (1)
\end{aligned}
$$

$$
{}^{i-1}T_i = \begin{bmatrix} c_{\theta_i} & -s_{\theta_i} c_{\alpha_i} & s_{\theta_i} s_{\alpha_i} & a_i c_{\theta_i} \\ s_{\theta_i} & c_{\theta_i} c_{\alpha_i} & -c_{\theta_i} s_{\alpha_i} & a_i s_{\theta_i} \\ 0 & s_{\alpha_i} & c_{\alpha_i} & d_i \\ 0 & 0 & 0 & 1 \end{bmatrix}
$$

When

$$
S_{\theta_i} = \sin(\theta_i) \quad , \quad C_{\theta_i} = \cos(\theta_i)
$$
$$
S_{\alpha_i} = \sin(\alpha_i) \quad , \quad C_{\alpha_i} = \cos(\alpha_i)
$$

The calculation from the initial reference position (A) to the end effector of the robot shown in Appendix A apply homogeneous transformation matrix (1). The end effector of the robot consists of F, H, R, and L represent, and the center of mass each link (Pcomi) of the robot. The homogeneous transformation matrix was shown as follows.

The transformation matrix between the initial reference frame (A) and the joint angle of right ankle (V) shown in Appendix D.1 is derived as:

$$ {}^{0}T_{V5} = {}^{0}T_{V1}\,{}^{V1}T_{V2}\,{}^{V2}T_{V3}\,{}^{V3}T_{V4}\,{}^{V4}T_{V5} \quad (2) $$

The transformation matrix between the initial reference frame (A) and the joint angle of right hip (q6) is derived as:

$$ {}^{0}T_{6} = {}^{0}T_{V5}\,{}^{V5}T_{1}\,{}^{1}T_{2}\,{}^{2}T_{3}\,{}^{3}T_{4}\,{}^{4}T_{5}\,{}^{5}T_{6} \quad (3) $$

The transformation matrix between the initial reference frame (A) and the left foot heel (F) is derived as:

$$ {}^{0}T_{14} = {}^{0}T_{6}\,{}^{6}T_{7}\,{}^{7}T_{8}\,{}^{8}T_{9}\,{}^{9}T_{10}\,{}^{10}T_{11}\,{}^{11}T_{12}\,{}^{12}T_{13}\,{}^{13}T_{14} \quad (4) $$

The transformation matrix between the initial reference frame (A) and each end effector of H, R, and L can repeat according to (4). Next, The calculation from the initial reference position (A) to the center of mass each link (Pcomi) of the robot. The transformation matrix was shown as follows.

The transformation matrix between the initial reference frame (A) and the COM of left hip (Pcom4) shown in Appendix D.3 is derived as:

$$ {}^{0}T_{C6} = {}^{0}T_{V5}\,{}^{V5}T_{1}\,{}^{1}T_{2}\,{}^{2}T_{3}\,{}^{3}T_{4}\,{}^{4}T_{5}\,{}^{5}T_{6}\,{}^{6}T_{7}\,{}^{7}T_{8}\,{}^{8}T_{9}\,{}^{9}T_{C5}\,{}^{C5}T_{C6} \quad (5) $$

The transformation matrix between the initial reference frame (A) and the center of mass each link (Pcomi) (i=1,2,3,5,..,11) of the robot can be obtained similar to (5). The Pcomi uses a measurement device, the researcher a development kinematics humanoid robot by using MATLAB are shown in Fig. 1(a).

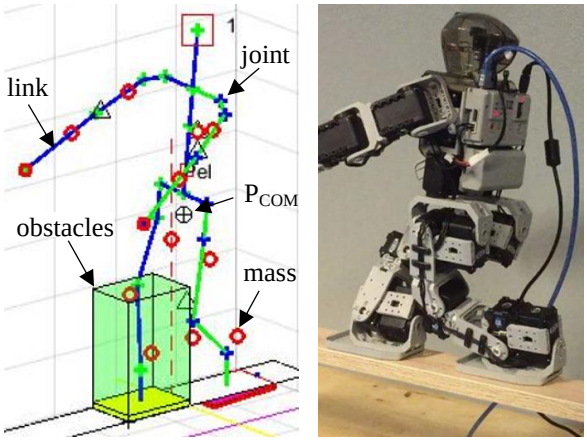

(a) (b)

Figure 1. The humanoid walking crossing a balance beam a) the simulation of humanoid robot b) the real humanoid robot

D. Stability

In general, there are two types of stability criteria that the trajectories of a biped mechanism depend on: static stability and dynamic stability. Static stability restricts the vertical projection of the center of the mass of the biped to the inside of the support polygon. The support polygon is defined as the area represented by the stance foot during the single-support phase (SSP) and the bounded area between the supported feet during the double-support phase (DSP) [6]. This work also proposes static stability, the robot can stop the walking motion any time without falling down. The robot walking on a narrow beam is that the motion is too slow.

E. Center of Mass (COM)

The position of the mass of each link was calculated to find the position COM of the robot in the rectangular coordinate frame as follows [1].

$$ P_{COM} = \frac{\sum_{i=1}^{n} m_i p_i}{\sum_{i=1}^{n} m_i} \quad (6) $$

When P_{COM}, m_i, p_i represent of position COM of the robot, a mass of each link, and position in the Cartesian coordinate frame of mass each link, respectively.

F. The Pattern Generators of Humanoid Robot Walking on a Narrow Beam

We present the humanoid robot and the pre-defined humanoid walking on a narrow beam gait that is used in the simulations and experiments in this section. We use this methodology in this paper to design a pre-defined walking gait.

The humanoid robot in the simulations has left leg set at the back and used as the swing leg. The right leg is the stance leg as shown in Fig. 1(a). So, the right leg obstructs the left one.

The support polygon is formed by its two feet. The size of each foot is 60 mm wide, and 100 mm long. The left and right feet are 50 mm apart for leg crossing. The stable DSP size 60 mm x 250 mm when two feet are crossed legs on the balance beam. The stable SSP size is 60 mm x 100 mm on the right foot. In this section, the balance control strategy is explained. The control strategy is divided into 5 steps as shown in Fig. 2.

Step1: The robot stands in balance. The left foot (LF1) follows the right foot (RF) (crossed legs) in Fig. 2 (a) which the position COG at the center of DSP1. The stability on the center of DSP1 size is 60 mm x 250 mm as shown in Fig. 2 (b).

Step2: The robot moves its body toward the right foot in Fig. 2 (c). The COG on DSP1 in right foot as shown in Fig. 2 (d).

Step3: The robot swings its left leg back forward and over the obstructing right foot as shown in Fig. 2 (e). The COG on center of SSP in the right foot (RF). The stability on SSP size is 60 mm x 100 mm as shown in Fig. 2 (f).

Step4: The robot leans its body forward and the left leg in front of the right leg as shown in Fig. 2 (g). The COG at the front of SSP in the foot right as shown in Fig. 2 (h).

Step5: The robot put the left foot (LF2) on the beam and in front of the right foot (crossed legs) as shown in Fig. 2 (i). The position of COG is at the center of DSP2. The stability on DSP2 size is 60 mm x 250 mm as shown in Fig. 2 (j).

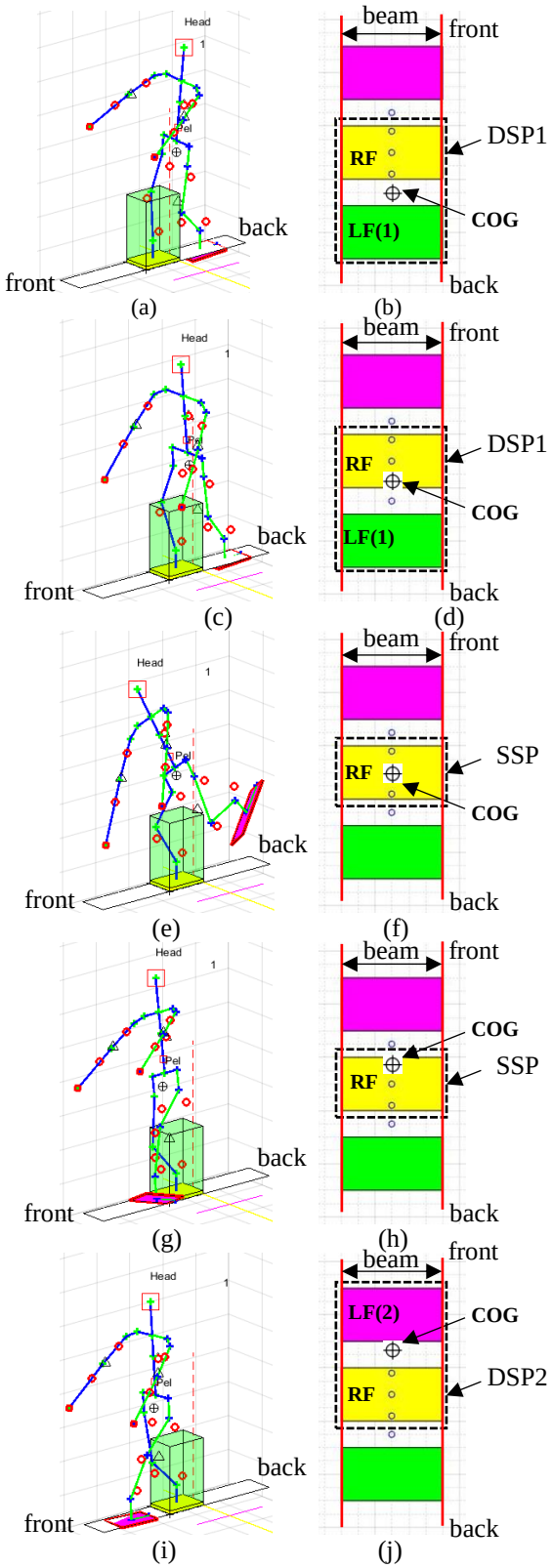

Figure 2. The control strategy is divided into 5 steps.

G. Trajectory

This research uses the trajectory of cubic spline interpolation for the trajectory of the joints of the robot. The velocity and acceleration of the initial and final conditions are set to zero. The interval time of cubic spline interpolation $[t_i, t_{i+1}]$ [19] can be rewritten as:

Position:

$$Q_{j,i}(t)=\frac{\ddot{Q}_{j,i}(t_i)}{6h_i}(t_{i+1}-t)^3+\frac{\ddot{Q}_{j,i}(t_{i+1})}{6h_i}(t-t_i)^3+\left(\frac{q_{j,i}}{h_i}-\frac{\ddot{Q}_{j,i}(t_i)}{6}h_i\right)(t_{i+1}-t)+\left(\frac{q_{j,i+1}}{h_i}-\frac{\ddot{Q}_{j,i}(t_{i+1})}{6}h_i\right)(t-t_i) \quad (7)$$

Velocity:

$$\dot{Q}_{j,i}(t)=-\frac{\ddot{Q}_{j,i}(t_i)}{2h_i}(t_{i+1}-t)^2+\frac{\ddot{Q}_{j,i}(t_{i+1})}{2h_i}(t-t_i)^2-\left(\frac{q_{j,i}}{h_i}-\frac{\ddot{Q}_{j,i}(t_i)}{6}h_i\right)+\left(\frac{q_{j,i+1}}{h_i}-\frac{\ddot{Q}_{j,i}(t_{i+1})}{6}h_i\right) \quad (8)$$

Acceleration:

$$\ddot{Q}_{j,i}(t)=\frac{\ddot{Q}_{j,i}(t_i)}{h_i}(t_{i+1}-t)+\frac{\ddot{Q}_{j,i}(t_{i+1})}{h_i}(t-t_i) \quad (9)$$

Jerk:

$$\dddot{Q}_{j,i}(t)=\frac{\ddot{Q}_{j,i}(t_{i+1})-\ddot{Q}_{j,i}(t_i)}{h_i} \quad (10)$$

The condition in velocity, acceleration of the initial and final are set to zero and continuous. Therefore, two extra knots (position $(\bar{q}_2,\bar{q}_{n-1})$) at time $\left(\bar{t}_2=\frac{t_1+t_3}{2},\bar{t}_{n-1}=\frac{t_{n-2}+t_n}{2}\right)$ [19], can be rewritten as.

$$\begin{aligned}\bar{q}_2&=q_1+h_1v_1+\frac{h_1^2}{3}a_1+\frac{h_1^2}{6}\ddot{Q}_{j,2}(t_2)\\ \bar{q}_{n-1}&=q_n-h_{n-1}v_n+\frac{h_{n-1}^2}{3}a_n+\frac{h_{n-1}^2}{6}\ddot{Q}_{j,n-1}(t_{n-1})\end{aligned} \quad (11)$$

When $Q_{j,i}(t), h_i=t_{i+1}-t, q_{j,i}, \ddot{Q}_{j,i}(t), v_1, v_n, a_1, a_n, j$ and i represent of position, interval time, position of joint, acceleration of joint, initial velocity, final velocity, initial acceleration, final acceleration, a joint of robot and a knot sequences, respectively. In the case of the trajectory COG position without j variable.

III. Numerical Simulation

The numerical simulation present step by step procedure of implementation of the proposed numerical simulation is outlined below:

- Step 1: The experiments pattern generators of humanoid walking on a narrow beam by trial and error method.
- Step 2: Create kinematics model of humanoid robot and test the model.

- Step 3: Calculate COM, COG, and two objective functions.
- Step 4: Process of meta-heuristic optimization Algorithm of Multi-objective by MOWOA, MOGWO, MOHS, and MOGA techniques.
- Step 5: The performance comparison meta-heuristic optimization based on the hypervolume (HV) indicator
- Step 6: Select the best of Pareto archive from best optimization algorithm of Multi-objective using the weighted sum method (WSM).
- Step 7: Return the best of Pareto archive and designed variables for experiments real humanoid robot.

The designated the position of COM ref for humanoid walks on a narrow beam indicating robot's stability are shown in Table IV.

TABLE IV. THE POSITION OF COM REF

Point	Time	COM ref x-axis (mm.)	COM ref y-axis (mm.)
P1	$0<t\leq t1$	110	-25
P2	$t1<t\leq t2$	110	10
P3	$t2<t\leq t3$	110	50
P4	$t3<t\leq t4$	110	90
P5	$t4<t\leq t5$	110	125

A. Multi-objective of Humanoid Robot Humanoid Walking on a Narrow Beam

The multi-objective optimization is a design assigned to determine the optimal point. For the problem that has more than one objective functions, it also has more than one optimum solution. The traditional combination of these results is called a set of Pareto optimal solutions or a Pareto front which is viewed in the objective function domain.

A typical mathematical formulation of multi-objective optimization can be expressed as:

$$Mimimze: F(x)=\{f_1(x), f_2(x),..., f_o(x)\} \quad (12)$$

Constraints

$$\begin{aligned} &g_i(x)\leq 0, i=1,...,m \\ &h_i(x)=0, i=1,...,l \\ &L_i\leq x_i\leq U_i, i=1,...,m \end{aligned} \quad (13)$$

When x and f_i represents of design variable and objective functions, respectively. Function $g_i(x)$ and $h_i(x)$ are the inequality and equality constraints while L_i and U_i are lower and upper bound constraints. Parameter m, l, and n are number of variable and o is number objective function.

B. Objective Functions

The designed trajectory of joints position on the robot for solve problem in this study. The designed variable of 18 joints, see (14). Two objective functions which are the maximum postural stability of a humanoid robot walk (minimum error of COM), minimum jerk. Details can be descripted as follows.

$$x=[q_1 \quad q_2 \quad \dots \quad q_{18}] \quad (14)$$

C. Error of COM Minimization

The result position of COM from calculate the objective is maximum postural stability (15), shown in Table IV which position of COM ref. The objective function can be calculated (15). It is shows robot walking stable on a narrow beam.

$$FOBJ1=\min\sum_{t=t_1}^{t=t_6}\left(\left|COM_X-COM_{Xref}\right|+\left|COM_Y-COM_{Yref}\right|\right) \text{ mm} \quad (15)$$

When $COM_X, COM_{Xref}, COM_Y, COM_{Yref}$ represent the position COM of x-axis in the designed variable of 18 joints, the position COM ref of x-axis in Table IV, the position COM of x-axis in the designed variable of 18 joints, the position COM ref of x-axis in Table IV, respectively.

D. Jerk Minimization

In this work, the servo motors are applied for the robot's joints, therefore, the system should have a minimum jerk, see (10), and objective function presents in (16) [20].

$$FOBJ2=\min\sum_{j=1}^{N}\int_{t_1}^{t_6}\left|\dddot{q}(t)\right|dt \quad (16)$$

The inequality and equality determined constraints for balance recovery as:

$$\begin{aligned} &q_{te_i}-10\leq q_{t_i}\leq q_{te_i}+10 \\ &SPD\leq COM\leq SPU \\ &V_{COM}\leq 50 \\ &P_{FL}\notin Ob \end{aligned} \quad (17)$$

When q_{t_i} is the value of joint angle range $\pm$ 10 degree from the joint (q_{te_i}) use trial-and-error method, The COM to remain inside support polygon. The support polygon down (SPD) is margin down of support polygon and the support polygon up (SPU) is margin up of support polygon, velocity of COM (V_{COM}) less than 50 mm/sec and the position of left foot (P_{FL}) outside obstacles (Ob) are show in Fig. 1(a).

E. Numerical Experiment

This investigation is conducted using MATLAB software. For each test system, 5 independent runs for each optimizer were operated, a comparative study of multi-objective meta-heuristics (MOMHs) for optimum design of humanoid robot humanoid walking on a narrow beam.

F. Non-dominated Solutions

In order to solve multi-objective problems the non-dominated solutions are identified an Pareto archive employs. The step by step procedure of implementation of the proposed algorithm is outlined below [13, 21]:

Step 1: Initialize population=90 of design variable vector is set as the joint angle of 18 joints for 5 periods (t_1-t_5).

$$Q=\begin{bmatrix} q_1 \\ q_2 \\ \vdots \\ q_n \end{bmatrix}=\begin{bmatrix} q_{1,1} & \cdots & q_{1,90} \\ q_{2,1} & \cdots & q_{2,90} \\ \vdots & \cdots & \vdots \\ q_{n,1} & \cdots & q_{n,90} \end{bmatrix} \quad (18)$$

When q is the value of joint angle range ± 10 degree from the joint use trial-and-error method. The angle is picked randomly and then roundup to the possible value of the Bioloid's angle. The servo motor of the robot has a resolution of 0.29 degree. The subscript n is the population size or number of search agents.

Step 2: Evaluate the fitness evaluation of a design variable vector. For the two objectives f_1, f_2 and the vector solution, F is feasible solutions in inequality constraints.

$$F(Q)=\begin{bmatrix} f_1(q_1) & f_2(q_1) \\ f_1(q_2) & f_2(q_2) \\ \vdots & \vdots \\ f_1(q_n) & f_2(q_n) \end{bmatrix} \quad (19)$$

Step 3: Determine the non-dominated solution (NS) as shown in Fig. 3. They store and update a set of non-dominate in Pareto archive (P).

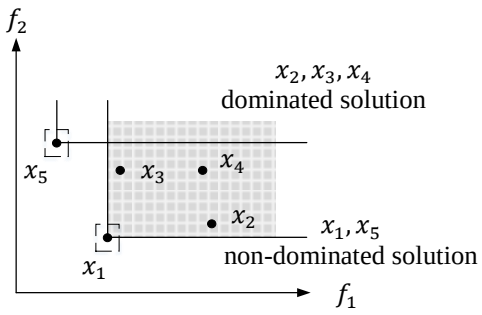

Figure 3. Non-dominated solutions.

Step 4: Select the best solution from Pareto archive using the roulette wheel technique and grid mechanism [12].

Step 5: Update the best solution if there are better solutions then the next generation is generated.

Step 6: Repeat step 1 to 5 until a termination criterion is met.

G. Hypervolume

The hypervolume is the volume (for 3D) or area (for 2D) covered by non-dominated solutions and measured with respect to a defined reference point (as shown in Fig. 4), which can be calculated as follow [13,14]:

$$HV=\sum_{i=1}^{n} V_i \quad (20)$$

Where HV is hypervolume, V_i is volume or area of hypercube, that is created by the i[th] non-dominated solution and reference point

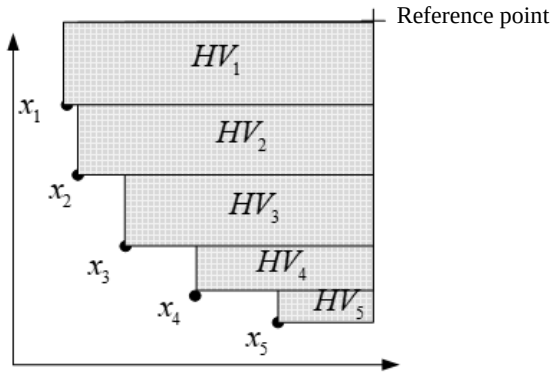

Figure 4. Area to calculate HV [14]

H. Multi-Criteria Decision Making (MCDM) methods

To select the best Pareto archive, the MCDM method, the weighted sum method (WSM) is utilized. The multi-criteria utility function (U) is introduced (21) [20].

$$U=\sum_{i=1}^{k} w_i F_i(x) \quad (21)$$

The objective functions may be converted to their normal forms as follows:

$$U=w_1\left(\frac{f_1(x)-f_1^{\min}}{f_1^{\max}-f_1^{\min}}\right)+w_2\left(\frac{f_2(x)-f_2^{\min}}{f_2^{\max}-f_2^{\min}}\right) \quad (22)$$

When $w_1, w_2, f_1(x), f_1^{\max}, f_1^{\min}, f_2(x), f_2^{\max}, f_2^{\min}$ represent the weight assigned to the first objective, the weight assigned to the second objective, the first objective function, maximize of the first objective function, minimize of the first objective function, the second objective function, maximize of the second objective function, minimize of the second objective function, respectively.

I. Parameter Settings

The general parameters of various algorithms such as the population size or number of search agents (n_a) = 30 , number of population (n_{pop}) = 90, the maximum number of iteration (n_{iter}) = 500, size of Pareto archive($n_{archive}$) = 300, number of grid per each dimension (n_{grid}) = 10, reference point (r_p)= 1.5 for the hypervolume, weight assigned to the first objective (w_1) =0.5 and weight assigned to the second objective (w_2) =0.5 for the weighted sum method (WSM), The other parameters specifically used by a particular optimizer are given below:

I. *Multi-objective Whale optimization Algorithm (MOWOA)* setting [12,13]: vector $\vec{\alpha}$ is linearly decreased from 2 to 0, a constant for defining the shape of the logarithmic spiral (b) = 1.

II. *Multi-objective Grey Wolf Optimizer (MOGWO)* setting [12, 13]: grid inflation parameter (alpha) = 0.1, leader selection pressure parameter (beta) = 4, and extra (to be deleted) repository member selection pressure (gamma) = 2.

III. *Multi-objective Harmony Search Algorithm (MOHS)* setting: harmony memory considering rate (hmcr) = 0.5, and pitching adjust rate (par) = 0.2.

IV. *Multi-objective Genetic Algorithm (MOGA)* setting [15]: crossing-over probability (pc) = 1.0, and mutation probability (pm) = 0.1.

J. Simulation Result

The multi-objectives tested function optimized by using proposed MOWOA, MOGWO, MOHS and MOGA comparative algorithms are shown in Fig. 5. These figures reflect the convergence quality of Pareto archive of optimization. The performance compared based on the hypervolume (HV) indicator. The reference point for calculating the hypervolume indicator, the maximum value the better algorithm. Results that obtained using algorithms MOWOA, MOGWO, MOHS and MOGA are reported in the Table V, MOGA is superior to the other. The best Pareto front obtained from this study is illustrated in Fig. 6, and the minimization weighted sum method (22), is 0.4366. The first objective function is 31.362 mm, and the second objective function is 3,540.068 deg/sec^3 as shown in Fig. 6. The designed variable is are shown in Table VI. The results of joint robot change trajectories is 12 joint (q1, q2, q3, q4, q5, q6, q8, q10, q12, q14, q16 and q18) and 6 joint (q7, q9, q11, q13, q15 and q17) is 0 degree all time. The joint start 1 sec to 5 sec.

TABLE V. HYPERVOLUME VALUES.

Algorithm	Minimum	Maximum	Mean	Std. Dev.
MOWOA	103,655.07	126,926.43	116,740.86	7,694.85
MOGWO	114,196.76	128,363.33	124,416.90	4,656.11
MOOHS	73,377.14	109,570.81	97,678.74	12,745.97
MOGA	129,241.40	**138,029.51**	134,284.77	2,860.78

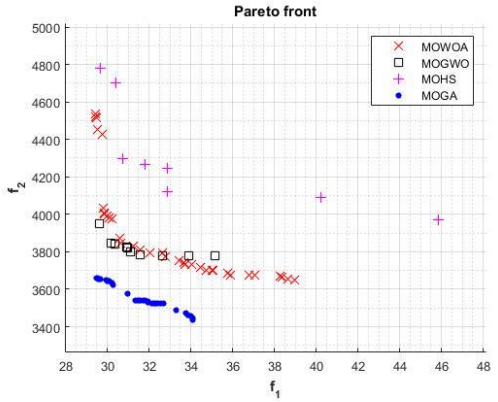

Figure 5. Best- obtained Pareto-front from each algorithm.

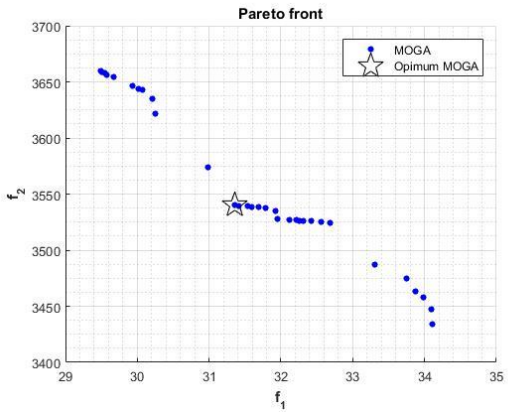

Figure 6. The best-obtained Pareto-front of MOGA and Optimum point.

TABLE VI. THE POSITION OF JOINT USE MOGA TECHNIQUES

Joint	t1	t2	t3	t4	t5
q1	0	-30.71	-73.35	-38.54	-24.94
q2	0	3.75	-14.95	66.59	81.49
q3	0	-29.28	18.28	-28.09	-39.73
q4	0	-0.02	-8.12	-10.72	-8.99
q5	0	28.33	60.71	66.24	75.11
q6	0	0.01	5.48	3.10	-3.19
q8	0	-0.00	-1.76	-4.36	-4.64
q10	0	11.13	-4.71	3.53	6.96
q12	0	1.39	-30.05	-26.82	-15.08
q14	0	2.92	-2.85	-3.24	-6.67
q16	0	-23.92	-52.91	20.53	39.73
q18	0	-4.97	12.91	57.27	54.81

IV. EXPERIMENTAL

From the previous section, the simulation shows that the humanoid robot on a narrow beam. Next step, the simulation results are implemented on the real humanoid robot.

A. Experimental Setup

This work uses the Bioloid premium Type A for all experiments. It is 350 mm tall, weight 1.736 kg, foot size is width 60 mm and length 100 mm. This commercial humanoid robot has 18 Degree of Freedoms (DOFs). The robot initial stable region inside 2 feet. The robot stands balance in the initial position. The left foot follow the foot right is 1 step (crossed legs) on beam size is width 60 mm and length 600 mm, shown in Fig. 7.

The robot system would keep joints position at the initial position (home position) at t_1 in Table VI. The main control unit for all 18 servo-motors is the CM-530 module through the RS232 communication protocol. The joint angle is acquired from CM-530 and send to MATLAB program the average sampling rate to 52.35 Hz.

B. Experimental of Humanoid Robot Walking Crossing a Balance Beam

As the simulation result indicates gives the best optimum point in Table VI. The movements of the robot are demonstrated in Fig. 2.The process of walking on a narrow beam can be divided into 5 periods. First period, the robot stands balance in the initial position inside 2 feet. The left foot follow the right foot is 1 step (crossed legs), see Fig. 7(A). Second period, the robot moved position COM to right foot, Fig. 7(B). Third period, robot walking left foot to forward, Fig. 7(C). Next, the left foot move lead right foot and move the robot body to forward, Fig. 7(D). Finally, the left foot touch the floor, as shown in Fig. 7(E).

The experimentation results of joint robot are compared; 1) the experiment results of joint robot on the real robot applying angle from trial-and-error method call "Trial-and-error"; 2) the experiment results of joint robot on the real robot applying angle from the best of optimum point simulation of MOGA method call "Actual"; 3) the result from the best of optimum point simulation of MOGA method call "Simulation". The joint robot change trajectories is 12 joint (q1, q2, q3, q4, q5, q6, q8, q10, q12, q14, q16 and q18) and 6 joint (q7, q9, q11, q13, q15 and q17) is 0 degree all time. The joint start 1 sec to 5 sec. as shown in Fig. 8, Fig. 9, Fig. 10 and Fig. 11.

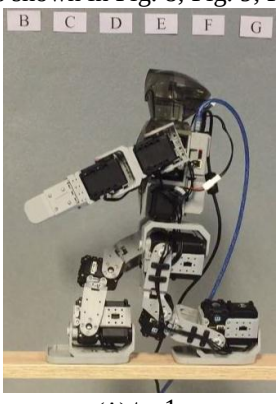

(A) t_1=1 sec

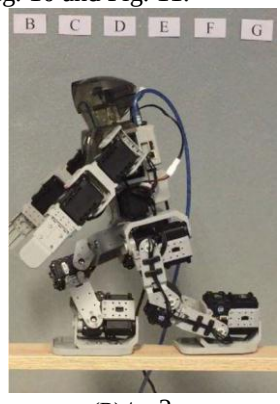

(B) t_2=2 sec

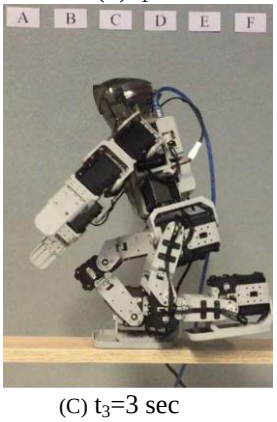

(C) t_3=3 sec

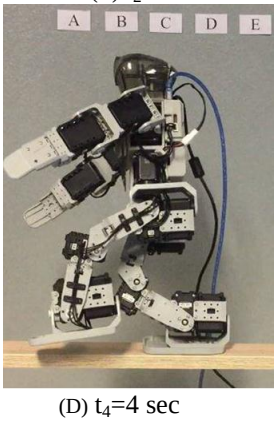

(D) t_4=4 sec

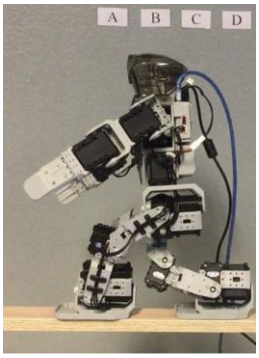

(E) t_5=5 sec

Figure 7. The experimental of humanoid robot walking crossing a balance beam.

TABLE VII. RESULT OF JERK FOR 3 TECHNIQUES.

Experimental	Jerk(degree/sec^3)
Trial-and-error	5,222.958
Actual	4,040.454
Simulation	3,540.030

TABLE VIII. COMPARISON RESULT OF JERK.

Experimental	Jerk
Trial-and-error VS **Actual**	22.64%
Trial-and-error VS **Simulation**	32.22%
Actual VS **Simulation**	12.38%

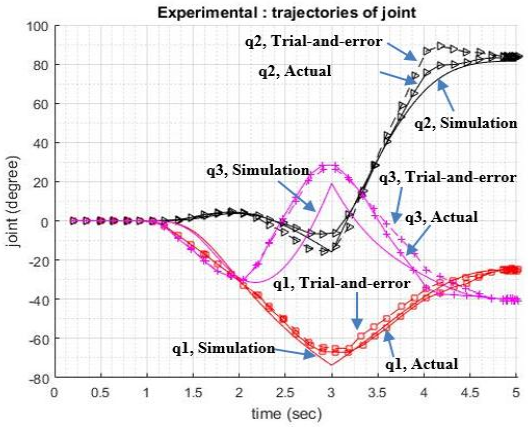

Figure 8. Comparison result of q1, q2, q3 for 3 techniques.

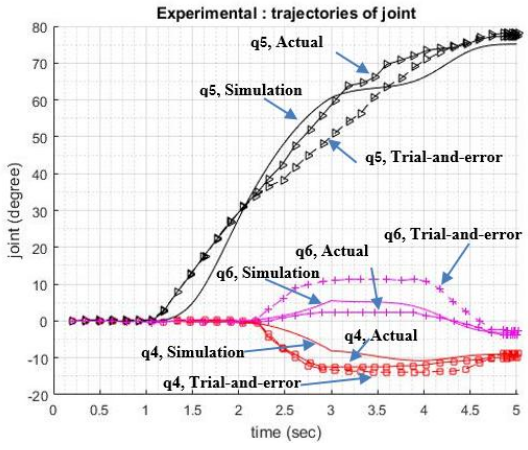

Figure 9. Comparison result of q4, q5, q6 for 3 techniques.

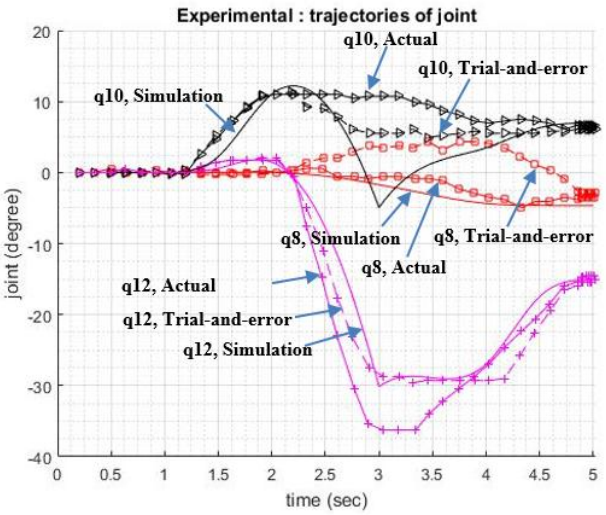

Figure 10. Comparison result of q8, q10, q12 for 3 techniques.

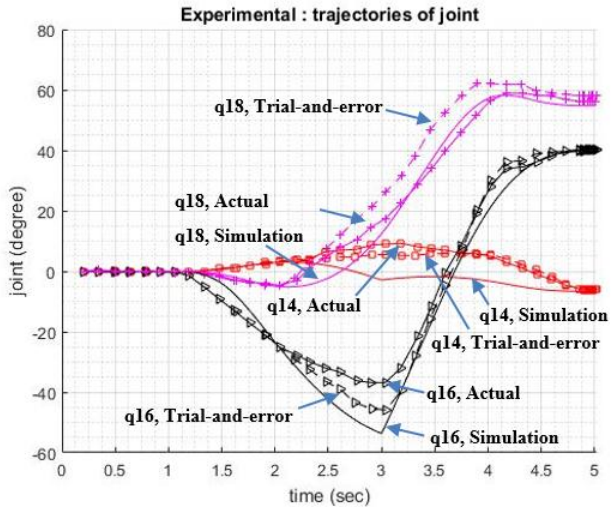

Figure 11. Comparison result of q14, q16, q18 for 3 techniques.

C. Results and Analysis

The calculated jerk of the experimental results yields the trial-and-error jerk is 5,222.958 degree/sec^3, while the actual one is 4,040.454 degree/sec^3, and the simulation yields 3,540.030 degree/sec^3, as presented in Table VII. By comparison of the jerks, the actual achieves 22.64%, less than the trial-and-error, and the simulation achieves 32.22% less jerk result than the trial-and-error. The simulation achieves 12.38% better result than the actual one as presented in Table VIII.

The result of the COG position must be considered to indicate the robot's stability. The experimental results determine the COG position, as show in Fig. 12. From the experiment, it is found that changing of COG position can be separated into 5 main parts including: 1) "P1" the period that the robot stands in balance which the COG on double-support phase (DSP1) in the left foot(1) following the right foot (crossed legs); "P2" is the period that the COG on double-support phase (DSP1) in the right foot; "P3" the period that the COG on center single-support phase (SSP) in the right foot when the robot moving the left foot forward; "P4" the period that the COG on forward single-support phase (SSP) in the right foot when the robot leans the body forward; and "P5" the period that the left foot (2) touches beam and the COG on double-support phase (DSP2) in the left foot(2) in front of the right foot (crossed legs), as shown in Fig. 12.

The experimental of COG trial-and-error result and actual result are inside the support polygon boundary (green line) all the time as shown in Fig. 13 and Fig. 14 thus sufficient stability margin is acquired. The average error of COG between the COG ref and experimental of trial-and-error result and actual result was calculated by root mean square (RMS). The average error of trial-and-error is 6.54 mm and the average error of the actual is 5.32 mm on x-axis. The actual result achieves 18.65% better result than the trial-and-error. The average error of trial-and-error is 18.08 mm and average error of actual is 16.55 mm on y-axis. The actual result achieves 8.46% better result than the trial-and-error. For the average error, the actual result achieves 13.55% better result than the trial-and-error average as shown in Table IX. For all results, they demonstrate that the techniques of optimization by MOGA can solve complexity problem, such as humanoid robot, better than the trial-and-error.

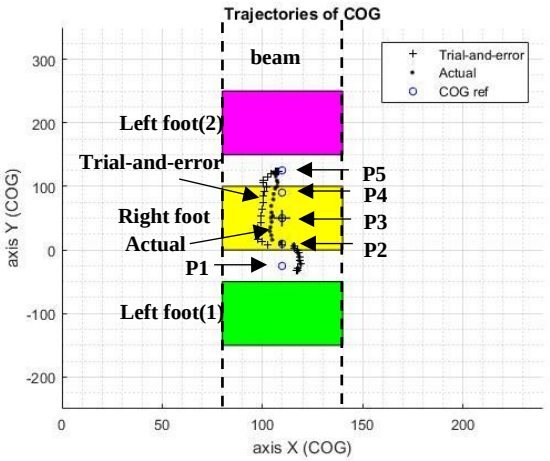

Figure 12. The experimental trajectory of COG.

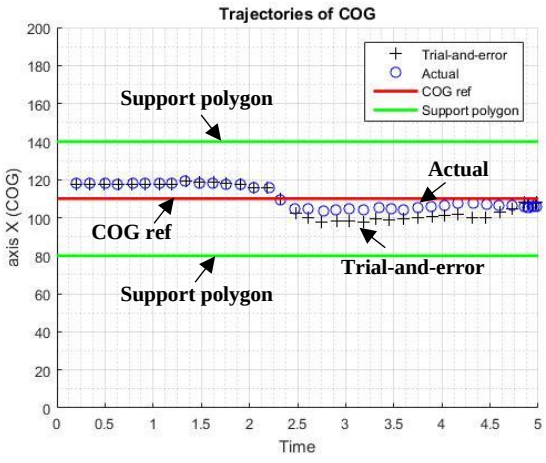

Figure 13. The trajectory of COG on x-axis in support polygon.

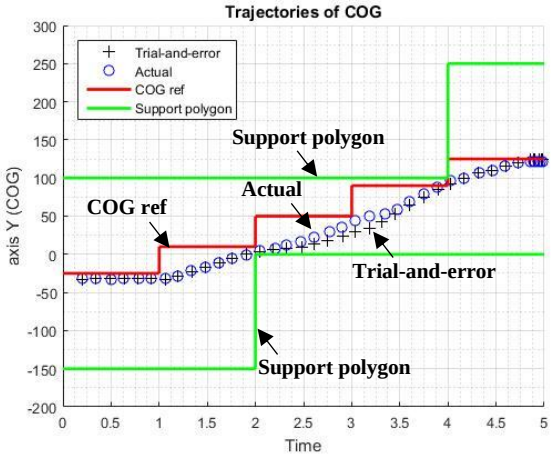

Figure 14. The trajectory of COG on y-axis in support polygon.

TABLE IX COMPARISON RESULT OF AVERAGE ERROR OF COG.

Experimental	Average error of COG by Root Mean Square (RMS)	
	x-axis (mm.)	y-axis (mm.)
Trial-and-error	6.54	18.08
Actual	5.32	16.55
%	18.65%	8.46%
	13.55%	

V. CONCLUSION

This paper proposes the methods of humanoid robot walking on a narrow beam. First, we discussed the motivation behind this research, and explained why the suggested strategy is needed. Second, we explained the balance control strategy. This control strategy uses static stability restricting the vertical projection of the center of the mass of the humanoid robot inside the support polygon. The experiments pattern was generated by trial and error method. Third, we verified the suggested control strategy using numerical simulations. The simulations of the humanoid robot (Bioloid premium Type A) used the MATLAB software. This work also proposes a comparative study of multi-objective meta-heuristics (MOMHs). Then the multi-objective tested functions were optimized by using proposed MOWOA, MOGWO, MOHS, and MOGA comparative algorithms. The performance was compared based on the hypervolume (HV) indicator. MOGA yields the best result. To select the best Pareto archive, the MCDM method, and the minimization weighted sum method (WSM) is 0.4366. The first objective function (error of COM minimization) is 31.362 mm, and the second objective function (jerk minimization) is 3,540.068 deg/sec^3.The resulting gait trajectory, COM and the position joint of humanoid robot. Finally, the position joint of simulation results of the best Pareto archive of MOGA are implemented on the real humanoid robot.

The experiments show the result of 2 objective functions. 1) The average error of COM between the COM ref and experimental of trial-and-error result and actual result was calculated by root mean square (RMS). The average error of actual result achieves 18.65% better result than the trial-and-error in x-axis, and the average error of the actual result achieves 8.46% better result than the trial-and-error for in y-axis. For average error, actual result achieves 13.55% better result than the trial-and-error average. 2) The jerk of experimentation results, the actual achieves 22.64% better result than the trial-and-error. The simulation achieves 32.22% better result than the trial-and-error, and the simulation achieves 12.38% better result than the actual. In summary, it was found that the techniques of optimization by MOGA can solve complex problem, such a humanoid robot, better than the trial-and-error method.

APPENDIX A. PARAMETER OF ROBOT

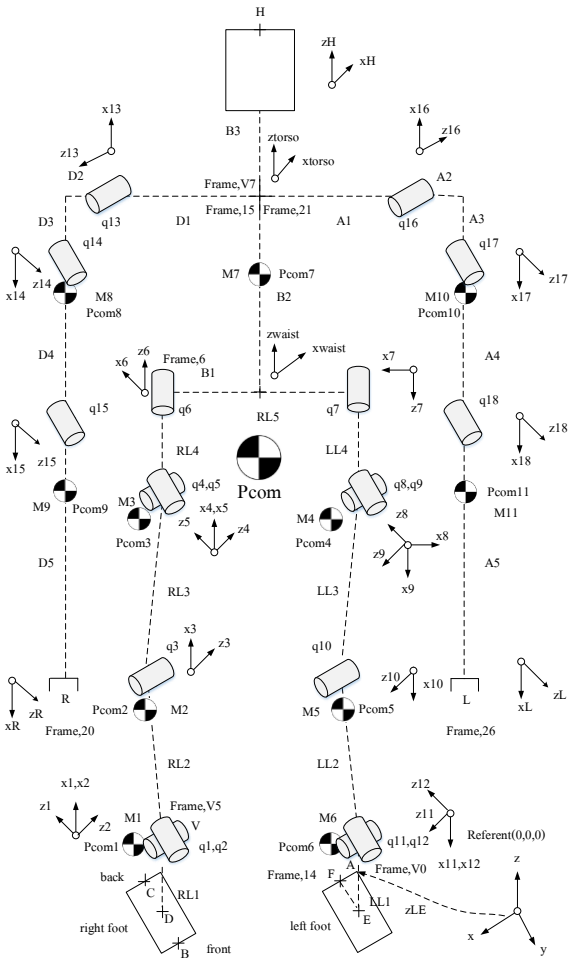

Figure A. Parameter of humanoid robot bioloid premium Type A.

APPENDIX B. VARIABLE AND CONSTANTS

Number	variable	Constants	Number	variable	Constants
1	LF0	110 mm.	14	A3,D3	14.5 mm.
2	LF1	100 mm.	15	A4,D4	67.5 mm.
3	LF2	50 mm.	16	A5,D5	106 mm.
4	RL1,LL1	31 mm.	17	L1COM,L9COM	-16.56 mm.
5	RL2,LL2	74 mm.	18	L2COM,L10COM	11.68 mm.
6	RL3,LL3	74 mm.	19	L3COM,L8COM	63.41 mm.
7	RL4,LL4	29 mm.	20	L4COM,L6COM	-18.25 mm.
8	RL5	80 mm.	21	L5COM,L7COM	-17.96 mm.

9	B1	40 mm.	22	L11COM	40.7 mm.
10	B2	31 mm.	23	L12COM	52.1 mm.
11	B3	49 mm.	24	L13COM	12.25 mm.
12	A1,D1	47 mm.	25	L14COM,L16COM	23.43 mm.
13	A2,D2	2 mm.	26	L15COM,L17COM	35.86 mm.

APPENDIX C. MASS OF EACH LINK

mass	Weight (kg.)
M1	0.172
M2	0.083
M3	0.166
M4	0.166
M5	0.083
M6	0.172
M7	0.582
M8	0.078
M9	0.078
M10	0.078
M11	0.078
total mass	1.736

APPENDIX D: DH PARAMETER

TABLE D.1 DH PARAMETER TABLE FROM POINT REFERENT (A) TO POINT JOINT RIGHT ANKLE (V)

Frame No.	θ_i	d_i	a_i	α_i
V1	pi/2	LF0	LF1	0
V2	pi+q_f	0	LF1	0
V3	pi+q_b	0	LF2	pi/2
V4	0	0	0	pi/2
V5	pi/2	0	RL1	pi/2

TABLE D.2 DH PARAMETER TABLE FROM POINT JOINT RIGHT HIP (q_6) TO POINT EFFECTOR OF HEAD (H).

Frame No.	θ_i	d_i	a_i	α_i
V6	q_6-pi/2	0	-B1	0
V7	0	-B2	0	0
V8	0	-B3	0	0

TABLE D.3 DH PARAMETER TABLE OF SUB MASS

Frame No.	θ_i	d_i	a_i	α_i	Pcom
C1	0	L1COM	L2COM	0	Pcom1
C2	q_2+$q_{i2,3}$	0	L3COM	0	Pcom2
C3	q_4+$q_{i4,5}$	0	0	pi/2	Pcom3
C4	0	L4COM	L5COM	0	
C5	0	0	0	pi/2	Pcom4
C6	0	-L6COM	-L7COM	0	
C7	0	0	-L8COM	0	Pcom5
C8	0	-L9COM	-L10COM	0	Pcom6
C9	q_6-pi/2	0	-L11COM	0	Pcom7
C10	0	-L12COM	0	0	
C11	0	0	0	pi/2	
C12	0	L13COM	0	0	
C13	q_{14}	0	L14COM	0	Pcom8
C14	q_{15}	0	L15COM	0	Pcom9
C15	q_{17}	0	L16COM	0	Pcom10
C16	q_{18}	0	L17COM	0	Pcom11

CONFLICT OF INTEREST

The author has received research grants from the Research and Development Institute, Loei Rajabhat University. The authors declare no conflict of interest.

AUTHOR CONTRIBUTIONS

I developed the theoretical formalism, performed the analytic calculations and performed the numerical simulations. And experiments at Dept. of Electrical and Electronic Engineering, Faculty of Industrial Technology Loei Rajabhat University, Loei, Thailand.

ACKNOWLEDGMENT

This work was supported by the Research and Development Institute, Loei Rajabhat University and Electrical and Electronic Engineering, Faculty of Industrial Technology Loei Rajabhat University.

REFERENCES

[1] S. Kajita, H. Hirukawa, K. Harada, K. Yokoi, *Introduction to Humanoid Robotics*, Heidelberg : Springer, 2014.
[2] S. Caron, Stair Climbing, "Stabilization of the HRP-4 humanoid robot using whole-body admittance control," *International Conference on Robotics and Automation (ICRA)*, pp. 277-283, 20-24 May 2019.
[3] N. Kaewlek, T. Maneewarn, "Inclined plane walking compensation for a humanoid robot," *International Conference on Control, Automation and Systems*, pp. 1403-1407, 27-30 October 2010.
[4] S. Kajita et al., "Biped walking pattern generation by using preview control of zero-moment point," *International Conference on Robotics & Automation*, pp. 1620-1626, 14-19 September 2003.
[5] J. Y. Kim, I. W. Park, J. H. Oh, "Walking control algorithm of biped humanoid robot on uneven and inclined floor," *Journal of Intelligent & Robotic Systems*, vol. 48, pp. 457-484, January 2007.
[6] H. F. N. Al-Shuka, F. Allmendinger, B. Corves, W. H. Zhu, "Modeling, stability and walking pattern generators of biped robots: A review," *Robotica*, vol. 32, pp. 907–934, September 2014.
[7] R. Tajima, D. Honda, K. Suga, "Fast running experiments involving a humanoid robot," *IEEE International Conf. Robotics and Automation*, Kobe Japan, pp. 1571-1576, 2009.
[8] S. Sakka and K. Yokoi, "Humanoid vertical jumping based on force feedback and inertial forces optimization," *IEEE International Conf. Robotics and Automation*, Barcelona Spain, pp. 3752-3757, 2005.
[9] E. Chiovetto, M. E. Huber, D. Sternad, M. A.Giese, "Low-dimensional organization of angular momentum during walking on a narrow beam," *Scientific Reports*, pp. 1-14, 8 January 2018.
[10] D. E. Orin, A. Goswami, S. H. Lee, "Centroidal dynamics of a humanoid robot," *Auton Robot*, pp. 161-176, 19 June 2013.
[11] R. J. Griffin, G. Wiedebach, S. McCrory, S. Bertrand, I. Lee, J. Pratt, "Footstep planning for autonomous walking over rough terrain," in *Proc. IEEE-RAS 19th International Conference on Humanoid Robot (Humanolds)*, pp. 9-16, 15-17 October 2019.
[12] K. Nuaekaew, P. Artrit, N. Pholdee, S. Bureerat, "Optimal reactive power dispatch problem using a two-archive multi-objective grey wolf optimizer," *Expert Systems with Application*, vol. 87, pp. 79-89, June 2017.
[13] K. Sanprasit and P. Artrit, "Optimal comparison using MOWOA and MOGWO for PID tuning of DC servo motor," *Journal of Automation and Control Engineering*, vol. 7, no. 1, pp. 52-56, June 2019.
[14] W. Chompoobud, S. Bureerat, N. Pholdee, "Multiobjective optimization of wind turbine blades-performance evaluation of some optimizers," *International Conference on Mechanical Engineering*, 13-16 December 2016.
[15] K. Nuaekaew, N. Pholdee, P. Artrit, S. Bureerat, "Comparative performance of multiobjective evolutionary algorithms for solving multiobjective optimal reactive power dispatch problems," *KKU Engineering Journal*, pp. 18-22, June 2016.
[16] R. N. Jazar, *Theory of Applied Robotics*, 2nd ed, New York, USA. : Springer, 2010.

[17] J. V. Nunez, A. Briseno, D. A. Rodriguez, J. M. Ibarra, V. M. Rodriguez, "Explicit analytic solution for inverse kinematics of Bioloid humanoid robot," *Brazilian Robotics Symposium and Latin American Robotics Symposium*, pp. 33-38, 2012.
[18] K. Omar et al., "Kinematic modeling of a humanoid soccer–player: Applied to BIOLOID premium type a robot," *Intelligent Robotics Systems : Ispiring the NEXT : 16th FIRA RoboWorld Congress, FIRA 2013*, Kuala Lumpur, Malaysia, London : springer, pp. 49-63, 2013.
[19] L. Biagiotti and C. Melchiorri, *Trajectory Planning for Automatic Machines and Robots*, Berlin Heidelbeng : Springer. 2008.
[20] P. Tangpattanakul, A. Meesomboon, and P. Artrit, "Optimal trajectory of robot manipulator using harmony search algorithms," *Recent Advances in Harmony Search Algorithm*, Virginia : Springer, pp. 23-36, 2010.
[21] I. R. Kumawat, S. J. Nanda, "Multi-objective whale Optimization," *IEEE TENCON Conf*, Penang, Malaysia, pp. 2747-2752, 2017.

Kittisak Sanprasit received his Ph.D. in Dept. of Electrical Engineering, Faculty of Engineering, Khon Kaen University, Khon Kaen, Thailand, in 2019. He is currently working as an Assistant Professor lecturer at Dept. of Electrical and Electronics Engineering, Faculty of Industrial Technology, Loei Rajabhat University, Loei, Thailand. His research interests include control systems and automation, humanoid robot walking and balancing robot.